A Comprehensive Approach to the Generation of Human-Like Arm Movements on Robot NAO

YUAN WEI [ID]
Vehicle & Transportation Engineering Institute, Henan University of Science and Technology, Luoyang 471000, China

e-mail: tsubasafx@foxmail.com

ABSTRACT Humanoid robot is one of the most active frontiers in robotics. As the basic part of motion of humanoid robot, human-like motion planning is always one of the research hotspots and difficulties. In this paper, a comprehensive approach is proposed to help robot NAO generate the human-like arm movements. Firstly, a novel arm motion mode is built based on the Movement Primitives (MPs). The whole arm movement can be decoupled into different simple sub-movements with different motion models, which improves the accuracy and computational efficiency of human-like arm movements. Then a motion decision algorithm based on Bayesian Network (BN) is proposed to help robot NAO choose the suitable motion model among these MPs. Finally, according to the structure features of the MPs, the IK solutions can be classified into two categories: methods based on index and on geometrical constraints. Through the comprehensive approach, the robot NAO can generate various human-like arm movements with satisfactory accuracy. The availability of the approach is verified by similarity experiment and human-like movement experiment.

I. INTRODUCTION

With the development of the robot technology and the expanding of the application area, new generations of humanoid robots are designed to interact and communicate with humans in a natural and friendly way [1]. The anthropoid shape gives humanoid robots the advantages over other robots in HRI and makes them more accessible for humans [2]. In HRI, humanoid robots work with humans and even can be the companion of humans. Thus, except for the anthropoid shape, humans prefer that humanoid robots have the manipulation ability like humans, so that they can perform various complex tasks [3]. The anthropomorphic arms provide humanoid robots powerful manipulation ability and the human-like arm movements is the motion foundation of the anthropomorphic arms. The research of the human-like arm movements determines whether or not the humanoid robots meet the requirements of the tasks in HRI. Meanwhile, through performing the tasks like humans, the robots can integrate into human life better and be trusted by humans [4].

The key issue of the human-like arm movements is to generate anthropoid arm postures [5]. The traditional methods

The associate editor coordinating the review of this manuscript and approving it for publication was Yongping Pan [ID].

predict arm postures by optimizing the Human Performance Measures (HPMs). The early researches are mainly based on psychophysical discomfort [6], [7]. This HPM indicates that the farther from the center angle, the more uncomfortable humans feel. The HPMs are then extracted through different disciplines. Zacharias *et al.* [8] used the rapid upper limb assessment (RULA) from ergonomic researches to determine the naturalness of arm postures. Rosell *et al.* [9] proposed the concept of ''principal motion directions'' to reduce the dimension of the search space in order to obtain results with a compromise between motion optimality and planning complexity. Zhao *et al.* [10] assumed that there exists a torsion spring along the elbow swivel axis. One end of it is attached to the vertical plane, and the other end is attached to the plane formed by the upper and lower arms. Using this equivalent model, the generation of trajectories of both end-effector and joints can be obtained. Dounskaia *et al.* [11] proposed a novel cost function that represents neural effort for joint coordination to generate the arm movements. Considering the single HPM always cannot satisfy the requirements of human-like movements, researchers try to use the multi-objective optimization methods. Yang *et al.* [12] constructed several HPMs to predict arm postures. The HPMs includes joint displacement, discomfort,

delta potential energy and visual displacement. Hugues *et al.* [13] proposed three HPMs (the inertia of base, the inertia of the end-effector and the velocity profile) and evaluated their impact on the human-like movements. Almasri *et al.* [14] proposed a HMP based on energy to generate the human-like movements. The HPM includes the gravitational potential energy and the kinetic energy. Different from using the methods based on HPMs, some researchers apply the human arm characteristics observed by other disciplines to IK algorithms. Caggiano *et al.* [15] observed the behavior of human writers and recognized the joints of shoulder and elbow should have higher mobility than that of wrist. Xie *et al.* [16] proposed a hypothesis named ''Target Arm Pose'' to interpret the natural motion of human arm. Baes on it, a new IK algorithm is proposed to generate the human-like arm movements. Tian *et al.* [17] built a lookup table about redundant joint to calculate the IK solutions. Kuo *et al.* [18] introduced the fuzzy approach to obtain the elbow height in different behaviors and solves a unique pair of the IK solutions.

Whether they are based on HPMs or arm characteristics, the methods do have drawbacks. The methods based on single HPM always cannot satisfy the requirements of the human-like movements. For multi-objective optimization methods, there may be uncertainty because of the weight influence among different HPMs. Although the arm characteristics can be extracted by many methods, its accuracy also needs to be proved. With the development of artificial intelligence, more and more novel methods are applied into human-like movements of anthropomorphic arms [19], [20]. Chaudhary *et al.* [21] proposed an adaptive neuro-fuzzy inference system to solve the complexity in a multi-DOF robotic arm. Banga *et al.* [22] solved the IK problems and optimized the whole system with the feed-forward ANNs and Bees Back propagation. Panagiotis *et al.* [23] used the BN to predict the motion among different primitives due to BN's unique strengths both in inference and in visualization. Ding and Fang [24] presented the concept of motion language to obtain the planned results for humanoid manipulators. Liu *et al.* [25] proposed a correspondence method named wrist-elbow-in-line to map key positions of human demonstrations to the real robot for obtaining a valid analytical inverse kinematics solution. Although these methods can generate human-like arm movements, they ignore the influence caused by arm models. In fact, human arm movements are complex [26], [27]. During the movement, arm states are changing constantly. Different numbers and combinations of joints form different arm states [28]. Human arms can perform different and complex tasks by coordination and cooperation of different joints. Thus, the arm motion models are multiple and varying.

The major contributions of this paper is proposing an approach for anthropomorphic arms to improve the accuracy and efficiency of human-like arm movements. In order to achieve this purpose, a motion model based on the MP is proposed to represent different human arm movements. Then the BN is used to predict motion. The motion variables are
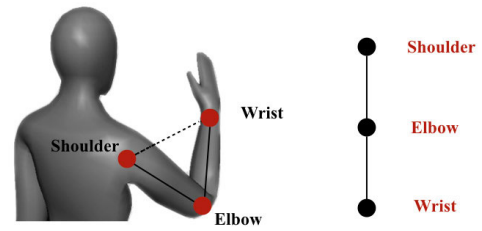

FIGURE 1. The skeleton-tree model.

FIGURE 2. The attributes of each joint.

extracted and the conditional dependencies are built. Finally, two types of IK solutions are proposed to generate the joint trajectories of anthropomorphic arms fast and accurately.

The remainder of this paper is organized as follows. In Section II, the arm motion model based on MPs is introduced. The motion-decision algorithm to help robot choose the suitable model among the different MPs is described in Section III. The corresponding different IK methods to solve the IK problems are shown in Section IV. Section V shows the results of experiments. Section VI concludes the paper.

II. MOVEMENT PRIMITIVE ORIENTED HUMAN ARM JOINT

A. KERNEL ACTION ELEMENT

In human arm joint space, complex arm movements are performed by the coordination of the shoulder joint, the elbow joint and the wrist joint. These joints can be described as a tree (see Fig. 1) and the nodes in the tree are series structures. In this tree, the shoulder, the elbow and the wrist represent the ancestor node, the parent node and the children node respectively. According to the characteristics of arm movements, each node has two motion attributes: 1) the position change relative to the world coordinate, 2) the orientation change relative to the former node. These two attributes are independent. For each node, these two motion attributes can occur simultaneously or respectively. When planning the arm movements, the shoulder joint is assumed immobile. Thus, the world coordinate is always fixed at the shoulder joint, and the shoulder joint only has the orientation attribute.

The attributes in the shoulder, the elbow and the wrist are shown in Fig. 2. Two kernel Action Elements (KAE) j, a are extracted from the tree model and the node attributes. $j \in G^{i \times 1}$

represents the joint vector, and i represents the number of joints. For arms, $i = 3$. $\boldsymbol{a} \in A^{1 \times 3}$ represents the attribute vector. The definitions of $\boldsymbol{j}$ and $\boldsymbol{a}$ are shown as follows:

$$\begin{cases} j = [S, E, W]^T \\ a = [P, R, PR] \end{cases} \quad (1)$$

The element S, E, W in $\boldsymbol{j}$ describe the different joints (shoulder, elbow and wrist) respectively and the element P, R, PR in $\boldsymbol{a}$ describe the motion attributes of joints (position change only, orientation change only, and both changes) respectively.

B. EXTRACTION OF MPS

As shown in Fig. 1, the elements in $\boldsymbol{j}$ can influence each other in order (from shoulder to wrist) because of the series structure. There are some extraction forms according to whether the joint is active or passive.

1) **element** A $\Rightarrow$ **element** B: the former is active and the motion attribute of the former can influence the latter's.
2) **element** A $\Rightarrow$ **element** B $\rightarrow$ **element** C: the element C is passive and moves with element B.
3) **element** A $\Rightarrow$ **element** B; **element** C: the element A and C are active.
4) **element** A: only the element A is active and does not influence the others' motion attributes.

For the same joint, the elements in $\boldsymbol{a}$ can be divided into two forms: simultaneous change (PR) and independent change (P or R). For different joints, the elements in $\boldsymbol{a}$ can also influence each other. Thus another two extraction forms can be obtained:

5) Generally, the orientation change of the former node will influence the position change of the latter node.

$$R_{former} \xrightarrow[\text{if change}]{\text{infuence}} P_{latter} : Former_R Latter_P$$

6) If and only if the orientation change of the ancestor node cannot influence the position change of the parent node, they will influence the attribute change of the alternate-generation node.

$$R_{ancestor} \xrightarrow[\text{if change}]{\text{not infuence}} P_{parent} : Ancestor_R Children_P$$

According to the extraction forms of the MPs above, a 3×3 matrix e called Primitive Matrix is proposed. The elements in Primitive Matrix are 1 or 0. Finally, through the Primitive Matrix e, the joint vector $\boldsymbol{j}$ and the attribute vector $\boldsymbol{a}$, the MPs can be extracted as follows:

$$MP_{form} = aej = \begin{bmatrix} P & R & PR \end{bmatrix} \begin{bmatrix} e_{11} & e_{12} & e_{13} \\ e_{21} & e_{22} & e_{23} \\ e_{31} & e_{32} & e_{33} \end{bmatrix} \begin{bmatrix} S \\ E \\ W \end{bmatrix} \quad (2)$$

C. REPRESENTATION OF MPS

The complex arm movements can be decomposed into different simple motion models through MPs, which makes great facilitation to generate human-like movements of anthropomorphic arms. According to (2), there are 10 MPs as shown in Table 1. Theses MPs can be divided into two types:

TABLE 1. Movement primitives.

Node	Primitives	Type
S	$S_R E_P W_P$	MMP
E	$E_R W_P$	MMP
S+E	$S_R E_{PR} W_P$	MMP
S+W	$S_R E_P W_{PR}$	MMP
S+W	$S_R W_P$	MMP
S+W	$S_R W_{PR}$	MMP
E+W	$E_R W_{PR}$	MMP
S+E+W	$S_R E_{PR} W_{PR}$	MMP
S	$S_R E_P W_R$	FMP
W	W_R	FMP

S, E and W represent the shoulder, the elbow and the wrist respectively. $S_R E_P W_P$ describes the movements that the orientation attribute of the shoulder and the position attribute of the elbow and wrist change. A similar explanation can be used in other primitives.

Motion Movement Primitive (MMP) and Function Movement Primitive (FMP). The MMPs describe the natural arm movements (the position of the wrist changes during the movements). The FMPs describe the obstacle avoidance movements (the position of the wrist is fixed during the movements). In this paper, we focus on the MMPs and the detailed explanations of the MMPs are shown as below:

1) $S_R E_P W_P$

Form: $S_R \Rightarrow E_P \rightarrow W_P$

Primitive Matrix: e= [0, 1, 1; 1, 0, 0; 0, 0, 0]

Explanation: the shoulder is active and the orientation change of the shoulder influences the position of the elbow. The wrist is passive and moves with the elbow. This MMP describes the movements that the arm moves around the shoulder.

2) $E_R W_P$

Form: $E_R \Rightarrow W_P$

Primitive Matrix: e= [0, 0, 1; 0, 1, 0; 0, 0, 0]

Explanation: the elbow is active and the orientation change of the elbow influences the position of the wrist. This MMP describes the flexion and extension movements of the elbow.

3) $S_R E_{PR} W_P$

Form: $S_R \Rightarrow E_P$; $E_R \Rightarrow W_P$

Primitive Matrix: e= [0, 0, 1; 1, 0, 0; 0, 1, 0]

Explanation: the shoulder and the elbow are both active. The orientation change of the shoulder influences the position of the elbow and the orientation change of the elbow influences the position of the wrist. This MMP describes the movements that are similar to reaching movements.

4) $S_R E_P W_{PR}$

Form: $S_R \Rightarrow E_P \rightarrow W_P$; W_R

Primitive Matrix: e= [0, 0, 0; 1, 0, 0; 0, 1, 1]

Explanation: the shoulder and the wrist are both active. The orientation change of the shoulder influences the position of the elbow. This MMP describes the movements that are similar to $S_R E_P W_P$. The only difference is that the orientation of the wrist changes actively when the wrist moves with the elbow.

5) $S_R W_P$
Form: $S_R \Rightarrow W_P$

    Primitive Matrix: e= [0, 0, 1; 1, 0, 0; 0, 0, 0]

    Explanation: the shoulder is active and the orientation change of the shoulder influences the position of the wrist. This MMP describes the alternate-generation movements. According to the extraction form (6), the orientation change of the shoulder cannot influence the position of the elbow but can influence the position of the wrist.

6) $S_R W_{PR}$
Form: $S_R \Rightarrow W_P$; W_R

    Primitive Matrix: e= [0, 0, 0; 1, 0, 0; 0, 0, 1]

    Explanation: the shoulder and the elbow are both active. The orientation change of the shoulder influences the position of the wrist. This MMP describes the movements that are similar to $S_R W_P$. The only difference is that the orientation of the wrist changes actively when the wrist moves with the shoulder.

7) $E_R W_{PR}$
Form: $E_R \Rightarrow W_P$; W_R

    Primitive Matrix: e= [0, 0, 0; 0, 1, 0; 0, 0, 1]

    Explanation: the elbow and the wrist are both active. The orientation change of the elbow influences the position of the wrist. This MMP describes the movements that are similar to $E_R W_P$. The only difference is that the orientation of the wrist changes actively when the wrist moves with the elbow.

8) $S_R E_{PR} W_{PR}$
Form: $S_R \Rightarrow E_P$; $E_R \Rightarrow W_P$; W_R

    Primitive Matrix: e= [0, 0, 0; 1, 0, 0; 0, 1, 1]

    Explanation: the shoulder, the elbow and the wrist are all active. The orientation change of the shoulder influences the position of the elbow and the orientation change of the elbow influences the position of the wrist. The orientation of the wrist changes actively. This MMP describes the movements that are similar to grasping movements.

D. FRAMEWORK BASED ON MPS
Through the MPs, the whole arm movement is decomposed into different sub-movements and these sub-movements occur in sequence. Thus, the MPs connect in series. The Fig. 3 shows the connection diagram of the MPs. The black circles represent different MPs and the arrows represent the occurrence sequence of the MPs. The semantics function $E(x)$ enriches the expressive patterns and the content of the MPs [29]. The decision function $F(x)$ is adopted to choose and connect the MPs. The detailed information will be shown in the next section.

    A motion framework based on the MPs is proposed. As shown in Fig. 4, the motion framework can be divided into four levels: a motion-decision level, a sub-movement level, a control level and a task level. The motion-decision level is the foundation of the motion framework and the MPs is the foundation of the motion-decision level. The left-to-right process (from the motion-decision level to the task level) is
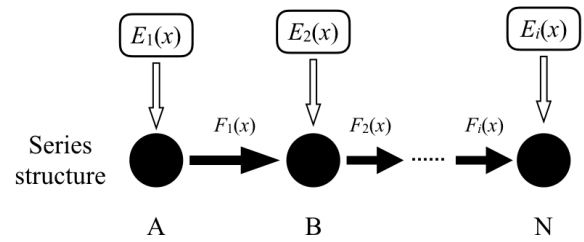
FIGURE 3. The connection diagram of the MPs.

a motion planning process of a specific task. If we want a robot to accomplish a specific task, the motion-decision level makes an analysis of the task and chooses different MPs to compose different sub-movements. Then the control model is chosen in the control level. Finally, through the interface between the algorithm and different manipulator platforms, the joint trajectories of a certain platform can be generated to accomplish the task. The left-to-right process (from the motion-decision level to the task level) is a self-learning process of a manipulator platform.

III. MOTION-DECISION ALGORITHM BASED BN
Through the MPs, the arm movements are decoupled to different motion models. According to different tasks, we need to choose suitable MPs from these models to help robots generate human-like movements. Thus, the choice of the MPs affects the accuracy of the human-like movements. The BN is a probabilistic graphical model that represents a set of random variables and their conditional dependencies via a directed acyclic graph. Due to its unique strengths both in inference and in visualization, the BN is widely used in the field of robotics. In this section, we propose a motion-decision algorithm based on BN. The motion variables are extracted and the prediction model is built. Through the motion-decision algorithm, the anthropomorphic arms can choose the suitable motion models according to different tasks.

A. MOTION VARIABLES
As shown in Fig. 2, the structure of the arm model is serial and each joint has two attributes: position and orientation. Thus, five motion variables S_R, E_P, E_R, W_P and W_R are extracted to build the BN model. These variables represent the position or orientation changes of the shoulder, the elbow or the wrist during the movements. Because the position of the shoulder is always fixed, the variable S_P is ignored. The motion capture system (Natural Point Inc., 8 Flex 13 cameras and 100 frames per second) is used to collect the human arm motion data and the priori probability of each variable can be obtained from these motion data. Then the conditional probability of each variable is determined. Each variable approximates to an exponential distribution. When the attributes of the joints are different, the expressions of the variables are different. The variables E_P, W_P are functions of the distance. The variable W_P is related to the difference between the distance from the shoulder position to the target position and the distance from the shoulder position to the
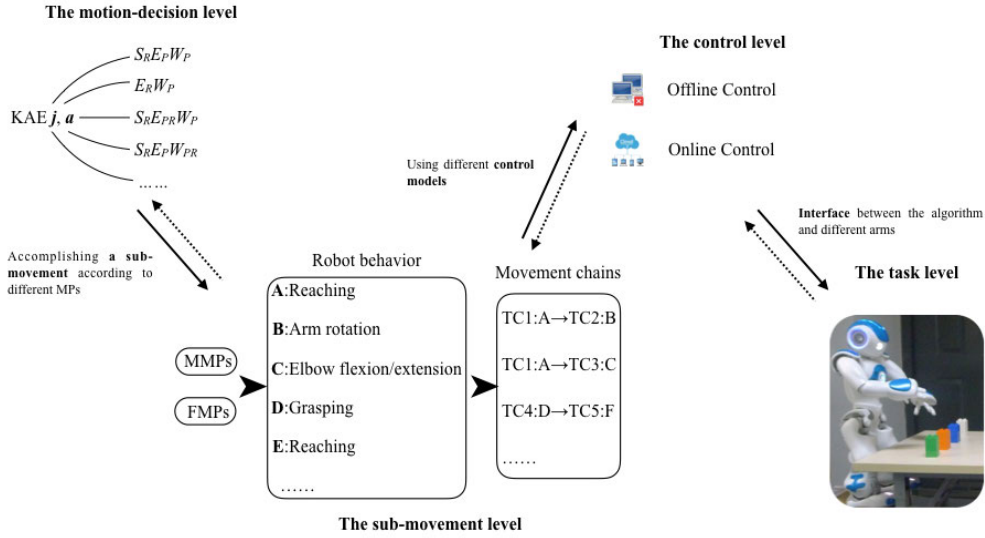
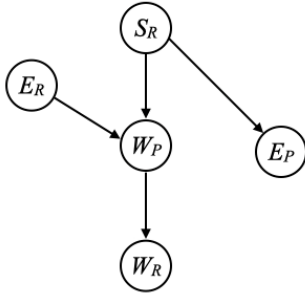**FIGURE 4.** The motion framework for anthropomorphic arms.

FIGURE 5. The BN represents the variables dependencies.

wrist position. The variable E_P is related to the difference between the distance from the elbow position to the target position and the length of the lower arm. The variables E_R, W_R are functions of the target orientation. Thus, the Exponential Probability Density Function (EPDF) is used to calculate the probabilities of these variables. Each variable has an EPDF associated with it. The rate parameter γ of each EPDF is calculated by maximum likelihood estimation method and the leave-one-out cross validation method. In this paper, the arm size of robot NAO is involved in the calculation of the EPDF. This method can be applied to other anthropomorphic arms by replacing the size.

B. DECISION MODEL

In this section, a BN, as shown in Fig. 5, is used to model the dependence relationships among the motion variables. The BN considers the prior information and sample data, and combines the subjective factors with objective factors, which can avoid the excessive use of data and bias caused by the subjective factors [30]. By inspecting the arrows in the BN, it is easy to determine which variable directly influences the others. A BN can be defined as follows:

$$B = (G, P) = (V, E, P) \tag{3}$$

where V represents a set of variables X_1, X_2, ..., X_n. E represents a set of directed edges between these variables. The joint probability distribution P can be written as follows:

$$P(X_1, X_2, \ldots, X_n) = \prod_{i=1}^{n} P(X_i | P_{ai}) \tag{4}$$

where P_{ai} represents the parent node of variable X_i.

Mutual information is a unit and is always used to measure the mutual dependence of the two variables. In order to decouple the movements, the mutual dependence of the two variables in every moment, not the whole movement process, needs to be determined. Thus, the Transient Mutual Information (TMI) is proposed to reflect the mutual dependence of the two variables in every moment during the movements. The expression of the TMI is shown as follows:

$$\hat{I}(X, Y) = P(x, y) \log \frac{P(x, y)}{P(x)P(y)} \tag{5}$$

where $P(x, y)$ is the joint probability distribution function for x, y. $P(x)$ and $P(y)$ are the marginal distribution probability functions for x, y. Similarly, the Transient Conditional Mutual Information (TCMI) is proposed and the expression is shown as follows:

$$\hat{I}(X, Z | Y) = P(x, y, z) \log \frac{P(x, y, z)}{P(x, y)P(z, y)} \tag{6}$$

In fact, the MPs consists of two or more variables. Thus, the Accumulative Mutual Information (AMI) is proposed to choose the suitable MPs. According to the node structure, the expressions of the AMI can be classified as a serial form and a parallel form. The expression of the serial form can be written as follows:

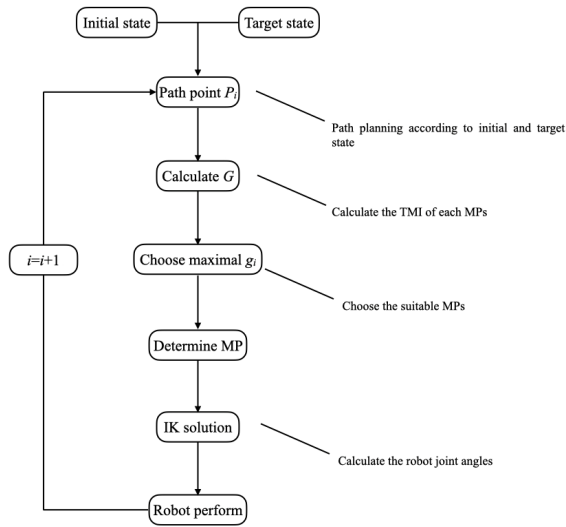$$I_s(v_1, v_2, \ldots v_i) = \hat{I}(v_1, v_2) + \hat{I}(v_2, v_3) + \ldots + \hat{I}(v_{i-1}, v_i) \tag{7}$$

FIGURE 6. The process of the motion-decision.

FIGURE 7. The result of the motion-decision at one moment.

FIGURE 8. The humanoid robot NAO.

where v_i represents different variables. The expression of the parallel form can be written as follows:

$$I_s(v_1, v_2, \ldots v_i) = \hat{I}(v_2, v_3|v_1) + \hat{I}(v_4, v_5|v_3) + \ldots$$
$$+ \hat{I}(v_{2i}, v_{2i+1}|v_{2i-1}) \quad (8)$$

where v_{2i+1}, v_{2i} represents different variables belonging to the same parent node.

Through (7) and (8), the AMI of each MP in every moment during the movements can be obtained. For example, the AMI function g of $E_R W_P$ is shown as follows and the other g of other MPs is similar to (9):

$$g = I_s(E_R, W_P) = \hat{I}(E_R, W_P) = P(E_R, W_P) \log \frac{P(E_R, W_P)}{P(E_R)P(W_P)}$$

$$= P(W_P|E_R)P(W_P|S_R) \log \frac{P(W_P|E_R)P(W_P|S_R)}{P(E_R)P(W_P)}$$

$$= \frac{P(W_P E_R)P(W_P S_R)}{P(S_R)P(E_R)} \log \frac{P(W_P E_R)P(W_P S_R)}{P(S_R)P^2(E_R)P(W_P)} \quad (9)$$

C. DECISION PROCESS

The Fig. 6 shows the motion-decision process. G is the set of the AMI function g_i and the dimension of G represents the decision results of the MPs. During the movements, the AMI values of different MPs can be calculated at every path point. Then the maximum g can be selected and the corresponding MP is the result of the motion-decision. After solving the IK problem, the robot can perform the task based on the selected MP.

$$G = [g_1, g_2, \ldots, g_m] \quad m = 1, 2, \ldots, 8 \quad (10)$$

In fact, as shown in Section II, every MP has a corresponding Primitive Matrix e. When the maximum g is selected, the corresponding Primitive Matrix can be obtained through (2). In order to visualize the result of motion-decision, the Primitive Matrix can be depicted graphically. Fig. 7 shows the state of the Primitive Matrix at one point. In Fig. 7, the horizontal ordinate represents the joint vector j and the vertical ordinate

represents the attribute vector a. There are two values 0 and 1 representing the activate state and the non-activated state respectively. The decision results at every moment can be displayed graphically through Fig. 7.

IV. COMPREHENSIVE APPROACH OF IK SOLUTION
A. ARM STRUCTURE OF HUMANOID ROBOT NAO

The humanoid robot NAO is used as the platform to verify the effectiveness of the method proposed in this paper. Fig. 8 shows the structure of NAO. Each arm of NAO has 5 DOFs (3 DOFs in shoulder, 1 DOF in elbow and 1 DOF in wrist). Although NAO only has 5 DOFs, its arm configuration is similar to the human arm. The DH parameters of NAO are shown in Table 2. After the data conversion between NAO and the real human arm, NAO can be used to generate the human-like arm movements accurately.

As shown in Section II, there are 8 MMPs representing the arm motion models. For NAO, each MP has different DOFs. According to structural features of different MPs, the IK problems can be divided into two methods: the method based on geometrical constrains and the method based on index.

B. METHOD BASED ON GEOMETRICAL CONSTRAINTS

When the robot NAO adopts some MPs such as $E_R W_P$ and $S_R W_P$, not all the joints of NAO are activated. Meanwhile, the orientation of the wrist does not change

TABLE 2. DH parameters of NAO arm.

i	α_i	a_i	d_i	θ_i
1	0	0	0	θ_1
2	$-\pi/2$	0	0	θ_2
3	$\pi/2$	0	L_u	θ_3
4	$\pi/2$	0	0	θ_4
5	$-\pi/2$	0	L_f	θ_5
T	0	0	L_t	0

TABLE 3. The motion information of the MPs.

MP	DOF	Motion forms	
		Shoulder	Elbow
$E_P W_P$	1		Flexion and extension
$S_R W_P$	1	Rotation	
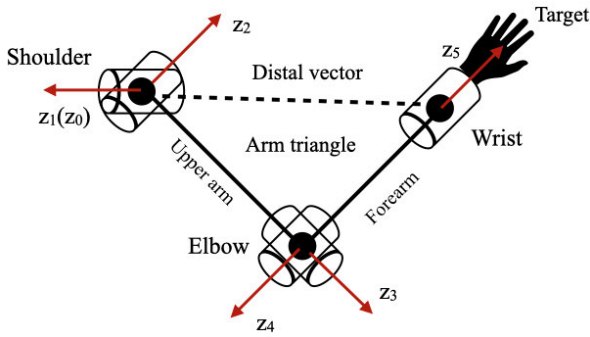
FIGURE 9. The arm triangle of the NAO.

FIGURE 10. The arm triangle for $E_R W_P$.

FIGURE 11. The arm triangle for $S_R W_P$.

during the movements. Thus, the motion of the wrist can be ignored when these MPs are adopted. The details about the motion information of the joints are shown in Table 3. In this paper, a concept *arm triangle* is introduced to visualize the arm configuration [31]. As shown in Fig. 9, the *arm triangle* is defined by the upper arm, the forearm and the distal vector. In the *arm triangle*, an arm movement can be determined by describing the change in the shape of the *arm triangle* together with its rigid rotation about the shoulder. The joint angles of the shoulder and the elbow can be obtained quickly according to the positions of the shoulder and the elbow.
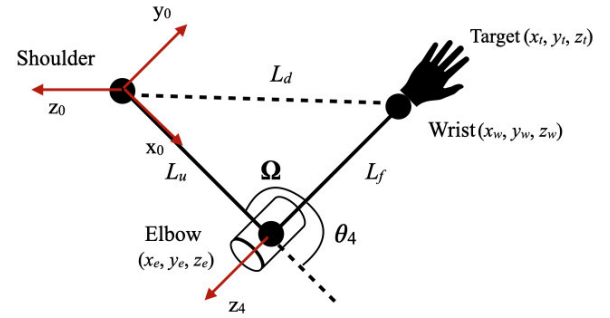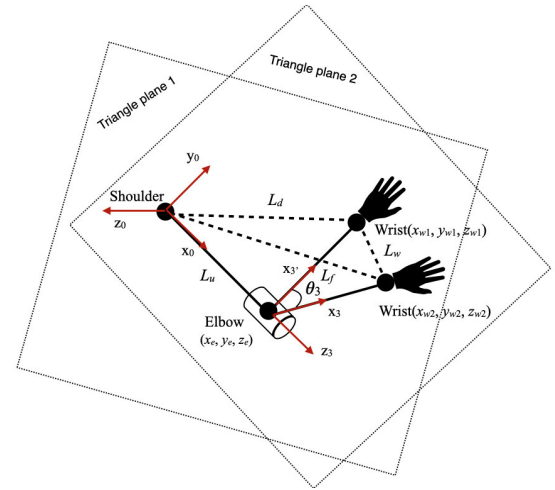
The MP $E_R W_P$ describes the flexion and extension movements of the elbow. Only joint 4 is activated and others do not change during the movements. So the *arm triangle* can be simplified as shown in Fig. 10. In this triangle, the shoulder is the origin. Meanwhile, because the joint angles do not change except for joint 4, the length of the upper arm, the forearm and the distal vector can be obtained. The angle between the upper arm and forearm can be obtained as follows:

$$\cos \Omega = \frac{L_u^2 + L_f^2 - L_d^2}{2 L_u L_f} \quad (11)$$

Thus the joint 4 can be calculated,

$$\theta_4 = \pi - \Omega \quad (12)$$

where L_u, L_f and L_d represent the length of the upper arm, the forearm and the distal vector respectively.

The MP $S_R W_P$ describes the alternate-generation movements and only one DOF of the shoulder participates in the movements. Fig. 11 shows the *arm triangle* for the MP $S_R W_P$. The shoulder is the origin and the position of the elbow does not change during the movements. Meanwhile, the positions of the wrist before and after the movement are given. Thus the joint 3 can be calculated as follows:

$$\theta_3 = \arccos \frac{2 L_f^2 - L_w^2}{2 L_f^2} \quad (13)$$

where L^f and L_w represent the length of the forearm and the distance between the wo positions of the wrist respectively.

C. METHOD BASED ON INDEX

Analytical solutions for other MPs are quite difficult to obtain. In this paper, the Gradient Projection Method (GPM) is adopted to solve the IK problems of these MPSs. The definition of the GPM is shown as follows:

$$\dot{\boldsymbol{\theta}} = \mathbf{J}^+ \dot{X} + k(\mathbf{I} - \mathbf{J}^+ \mathbf{J})\nabla H \quad (14)$$

where $\dot{\theta} \in R^n$ and $\dot{X} \in R^m$ are the joint and end-effector velocity respectively. $J \in R^{m \times n}$ is the Jacobian matrix, and $J+ = J^T (JJ^T)^{-1}$ is the Moore-Penrose generalized inverse of J. λ is a real scalar coefficient, and $I \in R^{n \times n}$ is the

identity matrix. H is the gradient vector of the HPMs to be optimized. The HPMs influence the accuracy of motion planning and the similarity of the human-like movements. According to the motion characteristics of each MP, these MPs can be divided into two types and the HPM of each type is also different.

The movements represented by $S_R E_{PR} W_P$ and $S_R E_P W_P$ can be described as reaching movements. In daily life, reaching movements are the most common arm movements. The minimum Total Potential Energy (TPE) is used as the HPM to explain how humans choose the natural arm postures during the reaching movement. The TPE includes the Gravitational Potential Energy (GPE) and the Elastic Potential Energy (EPE). The definition of the TPE is shown as follows:

$$f_{\text{TPE}} = f_{\text{GPE}} + f_{\text{EPE}} \quad (15)$$

The GPE can be calculated using the following formula:

$$f_{\text{GPE}} = m_u g h_u + m_l g h_l \quad (16)$$

where m_u and m_l represent the masses of the upper and the lower arm respectively. g represents the gravity acceleration. h_u and h_l represent the heights of the center of mass.

A virtual torsion spring model with variable stiffness is used to represent the EPE. The definition of the EPE is shown as follows:

$$f_{\text{EPE}} = \mu(\pi - \phi)^2/2 \quad (17)$$

where ϕ represents the elbow swivel angle. k represents the stiffness of the torsion spring. So the HPM for these MPs can be obtained.

$$H_R = m_u g h_u + m_l g h_l + \mu(\pi - \phi)^2/2 \quad (18)$$

Unlike $S_R E_{PR} W_P$ and $S_R E_P W_P$, the MPs $S_R E_P W_{PR}$, $S_R W_{PR}$, $E_R W_{PR}$ and $S_R E_{PR} W_{PR}$ consider the orientation change of the wrist. Thus the influence of the discomfort index should be considered on the basis of the TPE. The detailed definition is shown as follows:

$$\begin{aligned} f_{\text{NTPE}} &= f_{\text{TPE}} + \omega f_{wd} \\ &= m_u g h_u + m_l g h_l + \mu(\pi - \phi)^2/2 \\ &\quad + \omega(\theta_{wa} - \theta_{N,wa})^2 \end{aligned} \quad (19)$$

where ω is the weight coefficient of the discomfort and can be obtained by multiple regression methods. $\boldsymbol{\theta}_{wa}$ and $\boldsymbol{\theta}_{N,wa}$ represent the joint angle of the wrist and the center angle of the wrist respectively. The selected method of the center angle is shown in reference [31].

Meanwhile, the movements represented by these MPs can be described as grasping movements. In biophysics, the reaching movement is led by the upper arm and the lower arm plays a dominant role in the grasping movement [32]. Researches shows that the lower arm does more exercise and has lower inertia than the upper arm. So the minimum mobile distance of the elbow is used as the optimization function. The function can be written as follows:

$$\min s = \sqrt{(x_t - x_0)^2 + (y_t - y_0)^2 + (z_t - z_0)^2} \quad (20)$$
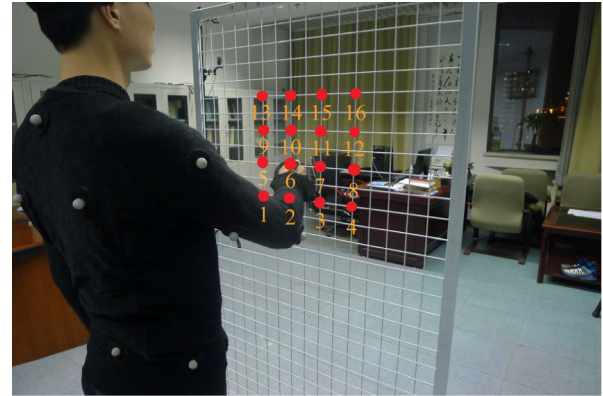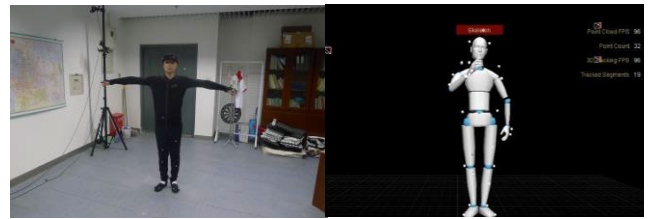

FIGURE 12. The similarity experiments.

(a)　　　　　　　　(b)

FIGURE 13. (a) Experimental equipment, (b) Operating software.

where (x_0, y_0, z_0) represents the initial position and (x_e, y_e, z_e) represents the target position. So the HPM for these MPs can be defined as follows:

$$H_G = k_1 s(d - \Delta d)/d + k_2 f_{\text{NTPE}}(q_{j=1,2,3,4,5})\Delta d/d \quad (21)$$

where k_1 and k_2 represent the weight coefficients. d and Δd represent the distance between the end-effector position and the target position. The difference is that d represents the distance when the arm comes into grasping moving state from reaching moving state and this distance is constant during the moment. While the distance represented by Δd is always changing during the grasping movement. $(d\text{-}\Delta d)$ and $\Delta d/d$ guarantee the smooth transfer of the reaching and grasping movements.

V. EXPERIMENT SETUP AND RESULTS
A. SIMILARITY EXPERIMENT
16 subjects with an average age of 21.5 (SD =1.16) voluntarily participate in the similarity experiments. As shown in Fig. 12, there are 16 points on the gridding and each subject is asked to reach these points in order. All the subjects are asked to hang down their arms naturally to be the initial arm posture. To avoid error caused by system and human factors, each subject needs to complete the arm movements at one point for 5 times. These 16 points are arranged in 4 rows and 4 columns and the interval of every two points is 10cm. The motion data of all the subjects are captured by motion capture system as shown in Fig. 13. As different in configuration between the human arm and NAO, the motion data captured by motion capture system should be normalized. The sailing method is adopted to transform these data [15]. After the data

TABLE 4. The motion information of the MPs.

Point	Experimental conditions			Movement Primitives							
	Subject number	test number	time (s)	$S_RE_PW_P$	E_RW_P	$S_RE_{PR}W_P$	$S_RE_PW_{PR}$	S_RW_P	S_RW_{PR}	E_RW_{PR}	$S_RE_{PR}W_{PR}$
P1	16	80	0.72	● red		● blue					● green
P2	16	80	0.58	● red							● blue
P3	16	80	0.6		● red						
P4	16	80	0.55				● red				
P5	16	80	0.8	● red		● blue					● green
P6	16	80	0.74	● red		● blue					● green
P7	16	80	0.57	● red							● blue
P8	16	80	0.55	● red							● blue
P9	16	80	0.94	● red		● blue					● green
P10	16	80	0.94	● red		● blue					● green
P11	16	80	0.93	● red		● blue					● green
P12	16	80	0.92	● red		● blue					● green
P13	16	80	1.01	● red		● blue					● green
P14	16	80	0.99	● red		● blue					● green
P15	16	80	0.93	● red		● blue					● green
P16	16	80	0.98	● red		● blue					● green

transformation, the real distance between the subjects and the points can be transformed to the distance between NAO and the points equivalently. When the sizes of the subjects are different, the initial positions of NAO are also different. Finally, these translated data can be regarded as the measure data to evaluate the proposed method.

In fact, because of the different positions of these 16 points, each subject reaches the different points with different MPs. For one same point, the arm states of the subjects are also different because of the different arm sizes of the subjects. During the experiments, the subjects adopt the same MP to reach one point no matter how many times the experiments are completed. Table 4 shows the experimental information of each point. As shown in Table 4, every point is carried out 100 experiments with 16 subjects. The time represents the mean time of all the subjects completing the experiments at the point. The mean time at different points is related to the distance between the point and the initial hand position of the subjects. The greater the distance, the longer the mean time. The MPs adopted by the subjects during the movements at different points are also different. In Table 4, the red circle, the blue circle and the green circle represent the occurrence sequence of the action. At some points there are two or three MPs happening during the movements but only one MP happening at other points. This is related to the position and orientation of the subjects during the movements. When the distance between the point and the initial hand position of the subjects is greater (such as the points in the first and second rows), the subjects adopt more MPs during the movements and the MPs are more similar. The MP $S_RE_PW_P$ always

happens firstly at most points, which further shows that the reaching movements are the most common arm movements. During the whole experiment, the MPs S_RW_P, S_RW_{PR} and E_RW_{PR} are not adopted in similarity experiments but will be adopted in human-like movement experiments. In Table 4, it can be seen that each MP represents a state of arm motion which can be regarded as the sub-movements. Finally, these sub-movements consist of the whole arm movements. Thus, the classification and recognition of arm movements play an important influence on human-like arm movements of anthropomorphic arms.

The robot NAO is also asked to reach these 16 points. The proposed method is adopted by NAO to verify the effectiveness. Through the motion-decision algorithm, NAO can select the suitable MPs autonomously and solve the IK problems by the IK methods in Section IV. Through the software Choregrahpe, the joint angles of NAO can be obtained. After the data transformation between NAO and the real human arm, the elbow position of NAO can be calculated through the converted path trajectories. These elbow positions are used to compare with the real elbow positions of the subjects during the experiments. The Fig. 14 and Fig. 15 shows the experimental results. Each subject completes the experiments on each point for 5 times and the average elbow position of each subject can be calculated during the experiments. The elbow positions of NAO are compared with these average elbow positions of all the subjects. There are 16 average errors on each point and each one of these 16 errors is the average error of one subject. In order to show these errors visually and quantitatively, the distribution illustration
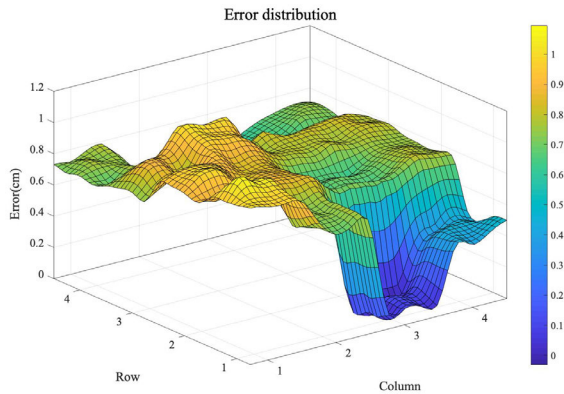
FIGURE 14. The elbow error distribution of all the subjects.

FIGURE 15. The average errors at 16 points.

of these errors is built as shown in Fig. 14. It can be seen that the errors on 16 points are all less than 1cm, which satisfies the accuracy requirements of human-like movements. The Fig. 15 shows the average errors of all the subjects on each point. Some interesting phenomena can be found in Fig. 15. When the whole movement is composed of more MPs, the error is always lager. There are three MPs at point 1, 5, 6, 9, 10, 11, 12, 13, 14, 15, 16, two MPs at point 2, 7, 8 and one MP at point 3, 4. The errors with three MPs (mean=0.7973, SD=0.1288) are larger than the errors with two MPs (mean=0.7167, SD=0.0416). The errors with only one MP (mean=0.26, SD=0.2404) are minimum. The reason is that the motion-decision model is built based on the sample data, so this model can reflect the general rules of arm movements. But this model cannot precisely predict where the MPs of different subjects change from one to another during the movements. The more number of the MPs during the movements, the more number of the state changing. Accordingly, the accumulative errors will increase. Meanwhile, it can be found that the errors are proportional to the distance between the positions of the points and the initial position of the subjects. The errors of the high rows (row 4: mean=0.6625, row 3: mean=0.8) are smaller than the errors of the lower rows (row 2: mean=0.8375). The reason is that when the distance is longer, the arm motion presents a steady state. Thus, the errors are relatively small. At Point 3, the method of solving the IK problems is the geometrical method, so the analytical solutions can be obtained. But there are still small error at this point because of the system errors.

B. HUMAN-LIKE MOVEMENT EXPERIMENT

Meanwhile, the robot NAO performs a human-robot collaboration experiment. Firstly, NAO takes the red block out of a subject's hand and sets it at the designated place. Secondly, NAO gives the green block on the desk to the subject. Then NAO takes the blue block out of the subject's hand and sets it at the designated place. Finally, NAO waves its hand and says "goodbye" to the subject. The experimental process is shown in the Fig. 16. Before the experiment, the subjects perform the same experiment and the motion data of the subjects
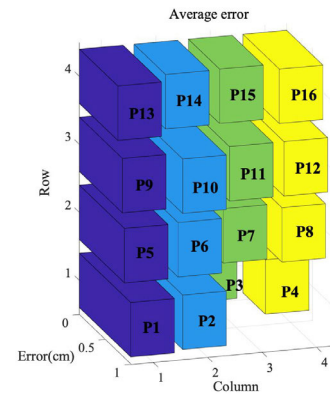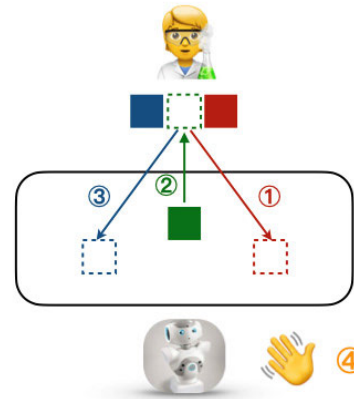

FIGURE 16. The process of human-like movement experiment.

are captured by motion capture system as the measure data. Some postures in the movement are regarded as the target postures. These data are also normalized and transformed to coincide with the configuration of the NAO arm. NAO is asked to stretch out its right hand horizontally as the initial posture to avoid the risk of collision between the arm and the desk. The motion information of NAO are shown in Fig. 17. Each picture shows the real action of NAO during the movement and the corresponding Primitive Matrix is at the top right corner of the picture.

Our method is compared with the Hierarchical Planning Strategy (HPS) [33] and the least norm algorithm. The indicator posture similarity S is used to evaluate these three motion planning algorithms. For a robot's posture H and a human's posture R, the distance between them is expressed as $dist(R, H)$. The shorter the distance is, the greater the similarity is, and vice versa. The posture similarity S is defined as follows:

$$S(R, H) = \frac{1}{1 + dist(R, H)} \quad (22)$$

The value of $S(H, R)$ is between (0,1]. When $dist(R, H) = 0$, that is, $S(H, R) = 1$, the similarity is the largest. The distance between two postures can be expressed by the Euclidean distance in N-dimensional space. Thus, the $dist(R, H)$ can
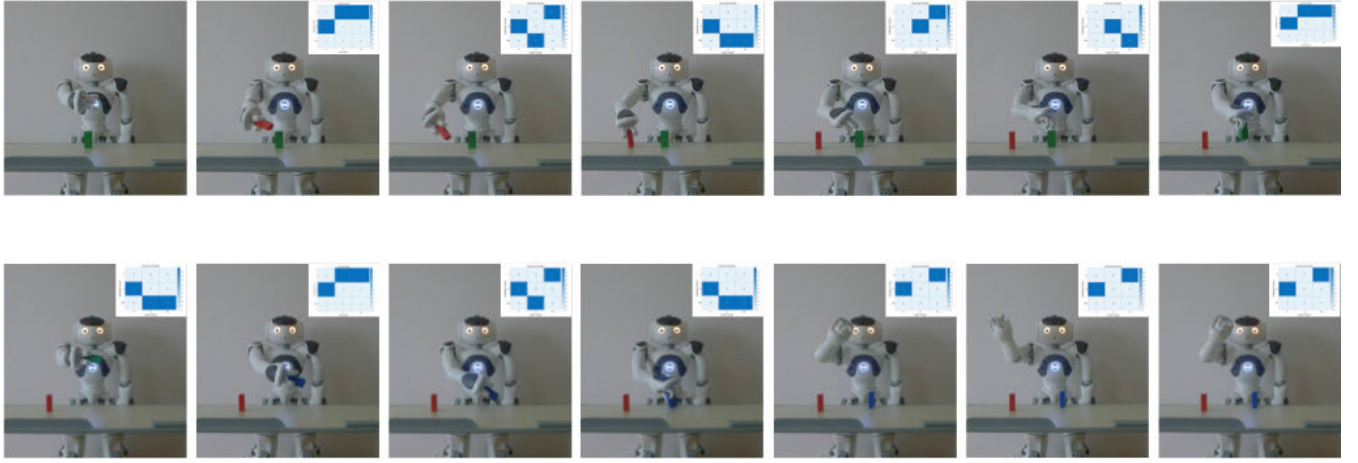
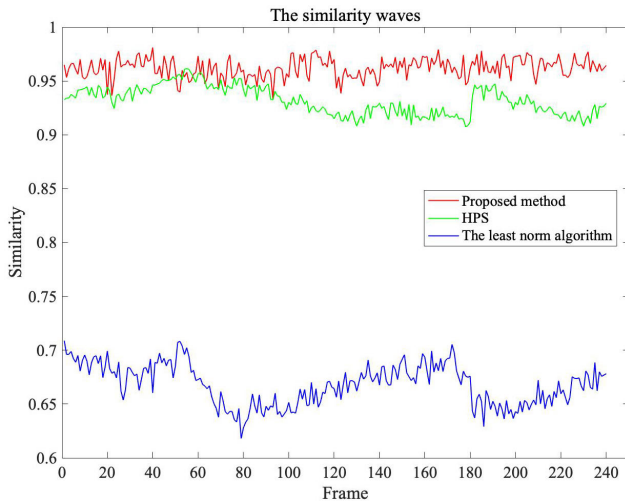**FIGURE 17.** The process of human-like movement experiment.

FIGURE 18. The similarity waves of three algorithms.

TABLE 5. The scores of two algorithms.

Method	Mean	Standard deviation
human-like algorithm	4.36	0.47
Least norm algorithm	2.12	*0.53*

HPS just decouples the arm movement according to motion features of different processes and ignores the influence of the arm models. Thus, the HPS cannot approximate the real arm models accurately. Especially when the movements are more complex, the errors of the HPS are larger. Compared with these methods, the proposed method shows the stronger ability to handle the human-like arm movements with multiple models. As a result, it can be concluded that the proposed method is useful for human-like motion planning of the anthropomorphic arms.

Meanwhile, when NAO performs the experiments, a total of 10 subjects are asked to observe NAO's actions and grade the human-like motions on their sense of security and comfort. After the experiments, subjects give the scores ranging from 1 to 5. The higher the scores, the safer and more comfortable the subjects feel. As a comparison, NAO performs the same task using the least norm algorithm and the subjects also grade the motions of NAO. The results are shown in Table 5. It can be shown that the scores of the proposed method are higher than the scores of the least norm algorithm, which proves the advantage of the proposed method in this paper.

VI. CONCLUSION AND FUTURE WORK
In this paper, a comprehensive approach is proposed to help robot NAO generate the human-like movements. In order to help robot mimic human arm movements accurately, a motion mode based on MPs is proposed. This model has definite physical meaning and reflects the inherent laws of human arm movements directly. According to human arm structures and joint motion features, ten MPs are extracted according to the extraction forms. These ten MPs are also classified into two types and applied to different situations. In fact, the experiments show that the states of the human arm change constantly during the movements. Not all the joints participant

be expressed as follows:

$$dist(\theta_r, \theta_h) = (\sum_{i=1}^{N} ||\frac{\theta_{ri} - \theta_{hi}}{\theta_{ri\_max} - \theta_{ri\_min}}||^2)^{\frac{1}{2}} \quad (23)$$

where θ_{ri} and θ_{hi} are the i-th joint angles of robot and human respectively. N is dimension of joint space. $[\theta_{ri\_min}\theta_{ri\_max}]$ is the angles range of the i-th joint.

The experimental results are shown in Fig. 18. The different color curves represent the similarity of these three algorithms respectively. The higher the values of the curve are, the nearer the predicted results approximate the real results. It can be shown that compared with the nonhuman-like algorithm (the least norm algorithm), both the proposed method and the HPS have the higher values. We also analyze the results of the proposed method and the HPS. At some stages, the values of the proposed method and the HPS are very close. This is because the models of the proposed method and the HPS are similar at these stages. But the errors of the HPS during the whole movements are higher than the errors of the proposed method because the

in the movements all the way. Thus, the decoupling of arm movements is important. Meanwhile, in order to represent the MPs visually and facilitate computations, the concept of the primitive matrix is proposed and the matrixes of different MPs are built. With this model, the robot can generate human-like movements accurately and fast.

After the decoupling of the arm movement, how to select a proper motion model under different tasks becomes an important issue. Thus, a motion-decision algorithm based on BN is constructed and can be applied to the human-like motion planning. The motion variables are extracted from the movements, and the motion models are obtained through the different combinations of motion variables. The probability of each MP is obtained by calculating the TMI, so the decision problem will turn into the optimization problem. With the motion-decision algorithm, the robot can choose an appropriate way to move automatically.

Finally, the IK problems can be solved through the structural features of the MPs. The DOFs of the MPs are different, so the method of solving the IK problems can be classified into two types according to whether the DOFs is redundant or not. For redundant structures, the human performance measures are proposed to predict the arm posture. For non-redundant structures, the analytical solutions can be obtained according to the geometrical constraints of the arm structure. When the robot performs the tasks, it can choose the corresponding model according to the MP selected by the motion-decision algorithm. The availability of the proposed approach is verified on humanoid robot NAO. The robot NAO performs two groups of experiments. Because of decoupling the arm motion, the accuracy of the human-like movements can be higher.

The proposed approach is an off-line method. All the motion data are calculated and then the robot performs the tasks according to these data. In the future work, we hope to propose an online method. Thus the future work will focus on the real-control human-like movements of the robot. In order to meet this requirement, the IK solution method also needs to be improved. Meanwhile, the MPs will be further divided to meet different situations.

REFERENCES

[1] S. Dong, Z. Yuan, X. Yu, J. Zhang, M. T. Sadiq, and F. Zhang, "Online gait adjustment for humanoid robot robust walking based on divergence component of motion," *IEEE Access*, vol. 7, pp. 159507–159518, 2019.

[2] F. Ficuciello, A. Migliozzi, G. Laudante, P. Falco, and B. Siciliano, "Vision-based grasp learning of an anthropomorphic hand-arm system in a synergy-based control framework," *Sci. Robot.*, vol. 4, no. 26, Jan. 2019, Art. no. eaao4900.

[3] D. Kulic, G. Venture, K. Yamane, E. Demircan, I. Mizuuchi, and K. Mombaur, "Anthropomorphic movement analysis and synthesis: A survey of methods and applications," *IEEE Trans. Robot.*, vol. 32, no. 4, pp. 776–795, Aug. 2016.

[4] S. M. M. Rahman, "Generating human-like social motion in a human-looking humanoid robot: The biomimetic approach," in *Proc. IEEE Int. Conf. Robot. Biomimetics (ROBIO)*, Dec. 2013, pp. 1377–1383.

[5] J. Qu, F. Zhang, Y. Wang, and Y. Fu, "Human-like coordination motion learning for a redundant dual-arm robot," *Robot. Comput.-Integr. Manuf.*, vol. 57, pp. 379–390, Jun. 2019.

[6] E. S. Jung and J. Choe, "Human reach posture prediction based on psychophysical discomfort," *Int. J. Ind. Ergonom.*, vol. 18, nos. 2–3, pp. 173–179, Sep. 1996.

[7] E. S. Jung, D. Kee, and M. K. Chung, "Upper body reach posture prediction for ergonomic evaluation models," *Int. J. Ind. Ergonom.*, vol. 16, no. 2, pp. 95–107, Aug. 1995.

[8] F. Zacharias, C. Schlette, F. Schmidt, C. Borst, J. Rossmann, and G. Hirzinger, "Making planned paths look more human-like in humanoid robot manipulation planning," in *Proc. IEEE Int. Conf. Robot. Autom.*, May 2011, pp. 1192–1198.

[9] J. Rosell, R. Suárez, C. Rosales, and A. Pérez, "Autonomous motion planning of a hand-arm robotic system based on captured human-like hand postures," *Auto. Robots*, vol. 31, no. 1, pp. 87–102, Jul. 2011.

[10] J. Zhao, B. Xie, and C. Song, "Generating human-like movements for robotic arms," *Mechanism Mach. Theory*, vol. 81, pp. 107–128, Nov. 2014.

[11] N. Dounskaia and Y. Shimansky, "Strategy of arm movement control is determined by minimization of neural effort for joint coordination," *Exp. Brain Res.*, vol. 234, no. 6, pp. 1335–1350, Jun. 2016.

[12] J. Yang, T. Marler, and S. Rahmatalla, "Multi-objective optimization-based method for kinematic posture prediction: Development and validation," *Robotica*, vol. 29, no. 2, pp. 245–253, Mar. 2011.

[13] O. Hugues, V. Weistroffer, and A. Paljic, "Determining the important subjective criteria in the perception of human-like robot movements using virtual reality," *Int. J. Humanoid Robot.*, vol. 13, no. 2, pp. 68–98, 2016.

[14] B. Almasri and F. B. Ouezdou, "Human-like motion based on a geometrical inverse kinematics and energetic optimization," in *Proc. IEEE/RSJ Int. Conf. Intell. Robots Syst.*, Sep. 2008, pp. 640–646.

[15] V. Caggiano, A. De Santis, B. Siciliano, and A. Chianese, "A biomimetic approach to mobility distribution for a human-like redundant arm," in *Proc. 1st IEEE/RAS-EMBS Int. Conf. Biomed. Robot. Biomechatronics (BioRob)*, Feb. 2006, pp. 393–398.

[16] B. Xie, J. Zhao, and Y. Liu, "Human-like motion planning for robotic arm system," in *Proc. 15th Int. Conf. Adv. Robot. (ICAR)*, Jun. 2011, pp. 88–93.

[17] Y. Tian, X. Chen, Q. Huang, and W. Zhang, "Kinematic analysis and solution of the natural posture of a 7DOF humanoid manipulator," in *Proc. IEEE Int. Conf. Autom. Logistics*, Aug. 2010, pp. 156–162.

[18] C.-H. Kuo, Y.-W. Lai, K.-W. Chiu, and S.-T. Lee, "Motion planning and control of interactive humanoid robotic arms," in *Proc. IEEE Workshop Adv. Robot. Social Impacts*, Aug. 2008, pp. 1–6.

[19] N. Garcia, J. Rosell, and R. Suarez, "Motion planning by demonstration with human-likeness evaluation for dual-arm robots," *IEEE Trans. Syst., Man, Cybern. Syst.*, vol. 49, no. 11, pp. 2298–2307, Nov. 2019.

[20] H. Su, W. Qi, and C.-G. Yang, "Deep neural network approach in human-like redundancy optimization for anthropomorphic manipulators," *IEEE Access*, vol. 4, pp. 124207–124216, 2016.

[21] H. Chaudhary and R. Prasad, "Intelligent inverse kinematic control of scorbot-er v plus robot manipulator," *Int. J. Adv. Eng. Technol.*, vol. 1, no. 5, pp. 158–169, 2011.

[22] V. Banga, R. Kumar, and Y. Singh, "Fuzzy-genetic optimal control for robotic systems," *Int. J. Phys. Sci.*, vol. 6, no. 2, pp. 204–212, 2011.

[23] P. K. Artemiadis, P. T. Katsiaris, and K. J. Kyriakopoulos, "A biomimetic approach to inverse kinematics for a redundant robot arm," *Auto. Robots*, vol. 29, nos. 3–4, pp. 293–308, Nov. 2010.

[24] X. Ding and C. Fang, "A novel method of motion planning for an anthropomorphic arm based on movement primitives," *IEEE/ASME Trans. Mechatronics*, vol. 18, no. 2, pp. 624–636, Apr. 2013.

[25] W. Liu, D. Chen, and J. Steil, "Analytical inverse kinematics solver for anthropomorphic 7-DOF redundant manipulators with human-like configuration constraints," *J. Intell. Robotic Syst.*, vol. 86, no. 1, pp. 63–79, Apr. 2017.

[26] A. V. Roitman, S. G. Massaquoi, K. Takahashi, and T. J. Ebner, "Kinematic analysis of manual tracking in monkeys: Characterization of movement intermittencies during a circular tracking task," *J. Neurophysiol.*, vol. 91, no. 2, pp. 901–911, Feb. 2004.

[27] S. Pasalar, A. V. Roitman, and T. J. Ebner, "Effects of speeds and force fields on submovements during circular manual tracking in humans," *Exp. Brain Res.*, vol. 163, no. 2, pp. 214–225, May 2005.

[28] M. Iacoboni, R. P. Woods, and M. Brass, "Cortical mechanisms of human imitation," *Science*, vol. 286, no. 5449, pp. 2526–2527, 1999.

[29] Y. Wei and J. Zhao, "Designing robot behavior in human robot interaction based on emotion expression," *Ind. Robot: Int. J.*, vol. 43, no. 4, pp. 380–389, Jun. 2016.

[30] L. A. Sierra, V. Yepes, T. García-Segura, and E. Pellicer, "Bayesian network method for decision-making about the social sustainability of infrastructure projects," *J. Cleaner Prod.*, vol. 176, pp. 521–534, Mar. 2018.

[31] S. Berman, D. G. Liebermann, and T. Flash, "Application of motor algebra to the analysis of human arm movements," *Robotica*, vol. 26, no. 4, pp. 435–451, Jul. 2008.

[32] C. Zobe, D. Krause, and K. Blischke, "Dissociative effects of normative feedback on motor automaticity and motor accuracy in learning an arm movement sequence," *Hum. Movement Sci.*, vol. 66, pp. 529–540, Aug. 2019.

[33] J. Zhao and Y. Wei, "A novel algorithm of human-like motion planning for robotic arms," *Int. J. Humanoid Robot.*, vol. 14, no. 1, 2017, Art. no. 1650023.

YUAN WEI received the B.S. degree from the Xi'an University of Technology, China, in 2011, and the Ph.D. degree from the Beijing University of Technology, China, in 2017. Since 2017, he has been a Teacher with the Vehicle & Transportation Engineering Institute, Henan University of Science and Technology, Luoyang, China. His research interest includes human-like motion of robotic manipulators.

● ● ●